Title

Time-Resolved Linear Dichroism Measurements of Carbonmonoxy Myoglobin as a Probe of the Microviscosity in Crowded Environments

Journal

The Journal of Physical Chemistry B, 121(29)

ISSN

1520-6106

Authors

Chen, Eefei
Kliger, David S

Publication Date

2017-07-27

DOI

10.1021/acs.jpcb.7b04107

Peer reviewed

THE JOURNAL OF PHYSICAL CHEMISTRY B

Article

pubs.acs.org/JPCB

Time-Resolved Linear Dichroism Measurements of Carbonmonoxy Myoglobin as a Probe of the Microviscosity in Crowded Environments

Eefei Chen and David S. Kliger*

Department of Chemistry and Biochemistry, University of California, Santa Cruz, California 95064, United States

Supporting Information

ABSTRACT: The distribution of viscosities in living cells is heterogeneous because of the different sizes and natures of macromolecular components. When thinking about protein folding/function processes in such an environment, the relevant (micro)viscosity at the micrometer length scale is necessarily distinguished from the bulk (macro)viscosity. The concentration dependencies of microviscosities are determined by a number of factors, such as electrostatic interactions, van der Waals forces, and excluded volume effects. To explore such factors, the rotational diffusion time of myoglobin in the presence of varying concentrations of macromolecules that differ in molecular weight (dextran 6000, 10 000, and 70 000), shape (dextran versus Ficoll), size, and surface charge is measured with time-resolved linear dichroism spectroscopy. The results of these studies offer simple empirically determined linear and exponential functions useful for predicting microviscosities as a function of concentration for these macromolecular crowders that are typically used to study crowding effects on protein folding. To understand how relevant these microviscosity measurements are to intracellular environments, the TRLD results are discussed in the context of studies that measure viscosity in cells.

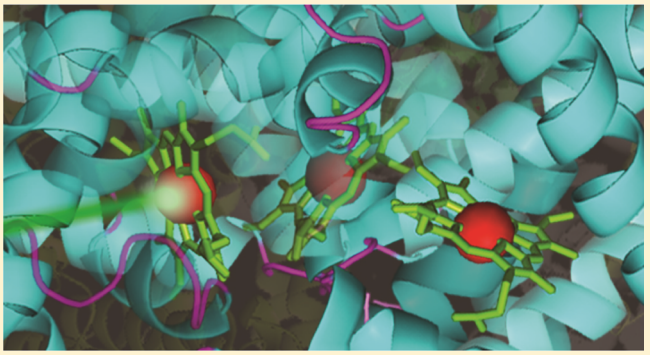

INTRODUCTION

Many studies have focused on elucidating determinants of protein folding or function in dilute protein solutions, an approach used to avoid aggregation phenomena that can take place in concentrated protein samples. However, under cellular conditions macromolecules (nucleic acids, complex sugars, other proteins) occupy about 40% of the cell's total volume, with protein concentrations varying from ∼10% in plasma to ∼30% in the erythrocyte cytosol (hemoglobin), and ∼50% in the mitochondrial matrix.[1−4] To understand the effect of such "crowded conditions" on protein folding, recent studies have added macromolecules at concentrations typically found in the cell to solutions that contain low concentrations of the protein whose folding is to be studied. Typical crowding agents include inert sugars, such as dextran or Ficoll, or protein crowders, such as bovine serum albumin (BSA) or lysozyme.

Molecular crowding conditions result in two significant influences—an excluded volume effect and relatively high viscosity, both governed by electrostatic and specific and nonspecific intermolecular interactions. In the excluded volume effect,[5−7] steric repulsions between molecules of highly populated solutions affect the volume available to other molecules and increase the total free energy of the system. Thus, the resulting effective concentration governs the thermodynamics and kinetics of protein (folding and function) and shifts the equilibrium toward states that maximize the available volume. Viscosity effects on protein folding have not been well studied. Here we determine the viscosities of solutions of macromolecular crowders to provide background information for future studies of viscosity effects on folding.

When considering viscosity effects of protein folding it is important to distinguish between macroviscosity, the viscosity of a bulk solution, and microviscosity, the viscosity at the micrometer length scale relevant to the protein (folding or function) of interest. That is, microviscosity monitors a probe's resistance to diffusion on a molecular scale, whereas macroviscosity is a measure of the diffusion of an infinitely large probe. The latter is typically measured using viscometers or rheometers, whereas microviscosity data largely have been obtained from rotational and translational diffusion times, measured with fluorescence correlation or anisotropy, ESR, and NMR spectroscopies, and fluorescent ratiometric or lifetime imaging with molecular rotors.[8−15]

The distribution of viscosities within the cell is heterogeneous because of the different sizes and natures of macromolecular components. As an example, based on protein concentrations alone, viscosities of the cytosol and the mitochondrial matrix should be significantly different. The concentration of enzymes

Received: May 1, 2017
Revised: June 19, 2017
Published: July 13, 2017

DOI: 10.1021/acs.jpcb.7b04107
J. Phys. Chem. B 2017, 121, 7064−7074

and other proteins in the mitochondrial matrix is so high that it is expected to markedly restrict solute diffusion.[16,17] How then do proteins that serve multiple functions in multiple cellular locations respond to different viscosities? Interestingly, studies of both the intramitochondrial matrix and the cytosol typically report viscosities (1−2 cP) that are not significantly greater than that of water.[18−26] Although most studies report measurements that are very similar within the particular cellular site, some do provide values that are vastly higher.[4,27−30] Possible explanations for such discrepancies include the characteristics and location of the viscosity probe, the cellular location actually probed, or binding of macromolecules to the probe.

Here, time-resolved linear dichroism (TRLD) spectroscopy is used to measure the rotational diffusion time of myoglobin (Mb) in solutions that vary in the concentrations of a variety of crowding macromolecules. Photodissociation of CO from carbon monoxide-bound myoglobin (MbCO) with a linearly polarized laser results in a spectral shift that makes it possible to monitor the time-dependence of linear dichroism (photoselection)[31] resulting from Mb rotational diffusion. The rotational diffusion process can be cleanly separated from chemical processes since the CO recombination reaction occurs on a much longer time scale (milliseconds) than the former (nanoseconds).

The results of these studies offer simple empirically determined linear and exponential functions useful for predicting the microviscosities experienced by proteins on the time and distance scales important for protein folding and functional processes. Furthermore, microviscosities as a function of concentration are tabulated for a number of macromolecular crowders that are typically used to study crowding effects on protein folding. These data will be useful for future studies that strive for a more detailed understanding of the effects of viscosity on protein folding. To achieve folded secondary structures, the distances traveled by a protein involve reorientation of localized segments. Thus, understanding rotational diffusion, which probes distances more relevant to intraprotein motions than translational diffusion, is more aligned with the goals of this study.

METHODS

Materials. Horse skeletal Mb, L-dextrans (D6, D10, and D70), Ficoll PM 70 (F70), D-fructose, and BSA (Sigma-Aldrich, St. Louis, MO), sodium phosphates (NaP, monobasic and dibasic), magnesium chloride ($MgCl_2$), and D-sucrose (Thermo Fisher Scientific, Waltham, MA), glycerol, and sodium hydrosulfite (dithionite) (Fluka Chemicals, Ronkonkoma, NY) were used without further purification.

Sample Preparation. For the TRLD experiments, ∼5 μL of 5 mM Mb (50 mM NaP, pH 7) was added to buffer solutions (pH 7) containing 50 mM NaP and D6 (20 concentrations from 50 to 490 mg/mL), D10 (18 concentrations from 60 to 430 mg/mL), D70 (17 concentrations from 50 to 480 mg/mL), Ficoll (25 concentrations from 26 to 480 mg/mL), BSA at pH 7 (14 concentrations from 50 to 450 mg/mL), BSA at pH 6.5 with 0.1 M $MgCl_2$ (24 concentrations from 30 to 460 mg/mL), sucrose (18 concentrations from 50 to 520 mg/mL), or glycerol (5 concentrations from 240 to 640 mg/mL) and deoxygenated with CO gas. After 30 min to 1.5 h, dithionite was added to form a solution of reduced MbCO with absorbance at 423 nm of ∼0.8 in a 5 mm path length cuvette.

A UV−vis spectrophotometer (UV-2102PC, Shimadzu, Columbia, MD or V750 JASCO, Easton, MD) was used to follow the integrity and concentration of the MbCO protein samples before, during, and after all experiments and to measure the spectra of the protein crowder buffers. The absorption values at 279 nm (BSA, ε_{279} = 43 824 M^{-1} cm^{-1}), obtained from the UV−vis spectra of the protein crowder buffers, were used to calculate their concentrations. Coupled with the corresponding refractive index values, these data were used to construct protein concentration calibration curves (See SI Figure S2 and Table S6). Refractive index values (ABBE-3L refractometer, Milton Roy, Raleigh, NC) were also used to generate calibration curves for inert crowder concentration determinations. The refractive indices of all samples were checked before and after the TRLD experiments. Adjustments of the pH for a final value of 7 were made with NaOH or HCl.

Macroviscosity Measurements. Solution macroviscosities were measured with a temperature-controlled (21 °C) Ostwald viscometer. The time (t, in seconds) required for the solution to traverse a known volume, a conversion factor (C) specific to the viscometer, and the solvent density (ρ) are used to calculate the viscosity (η) using the equation $\eta = C^*t\rho$. C and ρ were determined by calibration with water and by weighing known volumes of each solution, respectively. For all solutions, the values of parameters C, ρ, and η were determined from 3 to 5 trials. Standard deviations for the viscosity measurements were typically $\leq \pm 1\%$.

Rotational Lifetime Measurements. Rotational diffusion times were determined by TRLD measurements following photolysis of CO from MbCO with linearly polarized, 7 ns (full width at half-maximum), 22−23 mJ, 532 nm laser pulses from a Quanta Ray DCR-2A Nd:YAG laser (Spectra Physics, Santa Clara, CA). Because the Soret absorption band of MbCO is shifted relative to that of deoxyMb, and photolysis results in an oriented sample of Mb, the photolysis creates a linearly dichroic sample. This linear dichroism (LD) decays as the oriented Mb molecules randomize. The CO recombination times were measured by time-resolved absorption to be orders of magnitude longer (ca. 2 ms) than the rotational diffusion time of Mb (∼12 ns measured here), so the LD measurement is a good metric for rotational diffusion kinetics.

The TRLD measurements use an ultrasensitive LD method described previously.[32] Briefly, the sample is excited (in this case the Fe(II)-CO bond is photolyzed) by a laser with linear polarization oriented vertically. A 2 μs xenon flash lamp probe source passes through a linear polarizer to produce linearly polarized light oriented at +45° from vertical, through the sample, and then through a second linear polarizer oriented at −45° from vertical, and finally to a spectrograph and CCD detector gated to give a 5 ns detection window. By measuring the intensity of the probe beam, after rotating the second polarizer by a small angle, β, and then repeating the measurement after rotation of $-\beta$, as a function of time following laser excitation, LD can be determined by Signal = $[(I_{+45} - I_{-45})/(I_{+45} + I_{-45})] \approx \mathrm{LD}/\beta$. Here we used β = 0.014 radians.

To compensate for the rotation of the plane of polarized probe light by the cosolvents, a counter rotator (compensator) solution (D-fructose or D-sucrose) was positioned after the sample, but before the second, analyzing polarizer. The concentration of D-fructose or D-sucrose required to counter-rotate the plane of polarized light was calculated using the equation, [compensator] = [cosolvent]$([\alpha]_{\mathrm{D,cosolvent}}/[\alpha]_{\mathrm{D,compensator}})$. If necessary, the final compensator solution was fine-tuned by either diluting or concentrating the solution until the LD baseline was at zero.

TRLD data for MbCO were measured at 27 logarithmically spaced time points between 2.5 ns and 10 μs after photolysis of

DOI: 10.1021/acs.jpcb.7b04107
J. Phys. Chem. B 2017, 121, 7064−7074

the CO ligand. Between 10−16 data sets, comprising 100 averages at each time delay, were measured under each different cosolvent condition. The temperature of the sample was maintained at 21 °C during the experiments.

Data Analysis. Rotational diffusion lifetimes were determined from the TRLD data using singular value decomposition (SVD) and global kinetic fitting algorithms written in the mathematical software package Matlab (The MathWorks, Inc., South Natick, MA). SVD and global kinetic fitting have been described extensively in previous publications and so will not be discussed here.[33] The concentration and viscosity dependence of the rotational diffusion times were analyzed using Sigmaplot (Systat Software, Inc., San Jose, CA). Residuals obtained for the fits of the data were normalized to the corresponding values of the rotational diffusion lifetimes.

TRLD data measured in the presence of each crowder were fit to exponential $f = y_0 + a(\exp(bx))$, as well as linear, functions. In the latter, the results were analyzed to find the minimum number of linear sections that would best fit the data. These sections are characterized by polymer behavior in dilute, semidilute, and concentrated solutions (*vide infra*). The assignment of transition concentrations was based initially on determination of approximate transition points by inspection. Subsequently, linear fits were obtained for concentration ranges that progressively moved away from this apparent transition point. For example, for D70 solutions the lower concentration TRLD data were fit from 0−21%, 0−25%, and 0−30%. Comparison of the residuals (not shown) and the coefficient of determination (R^2) values (0.8984, 0.8675, 0.8220) for the fits gives the best transition concentration; in this case, 21%.

Viscosities were calculated from the rotational diffusion times (τ) obtained from TRLD measurements using the Stokes-Einstein-Debye relationship. Because TRLD measures rotational movements on the molecular distance scale, the viscosity calculated is actually the microviscosity (μ_η) experienced by the test protein myoglobin. Therefore, $\mu_\eta = 3kT\tau/(4\pi R_h^3)$, where R_h is the hydrodynamic radius of myoglobin, k is the Boltzmann constant, and T the temperature. These calculated microviscosities are compared (in the SI) to those calculated using equations reported from absorption anisotropy and multiphoton fluorescence correlation experiments, two studies that use some macromolecular crowders that overlap with those used here.[12,34]

Crowder Characteristics. The crowding macromolecules used in this study differ in size, shape, molecular weight, and charge. The dextrans used have molecular weights (MW) of 70 000, 10 000, and 6000 g/mol. The MW for protein crowder BSA is 66 463 g/mol and the small cosolvents glycerol and sucrose have MW's of 92.1 g/mol and 342.3 g/mol. The size of these cosolvents are described by the Stokes and hydrodynamic radii (ρ_h, R_h) for D70, D10, sucrose, and BSA—58 Å,[35] 23.6 Å,[35] 5.1 Å,[36,37] and 39.2 Å,[38] respectively.

Zeta potential (ζ), which is a metric for the attraction/repulsion between charged surfaces, can be influenced by changing solution pH or the ionic strength. When ζ of a solution is zero, the pH of that solution is the isoelectric point (pI). ζ values for BSA under conditions used in these TRLD studies were obtained from literature. For BSA, ζ values were −10 to −14 (NaP, pH 7) and about −3 (0.1 M $MgCl_2$, pH 6.5).[38−42] In the presence of 0.1 M $MgCl_2$, pI is pH 4.7 and in 15 mM NaP without salt the pI is ∼pH 4.95.[38,39] Table S1 includes all the characteristics of the crowders that are important for this study.

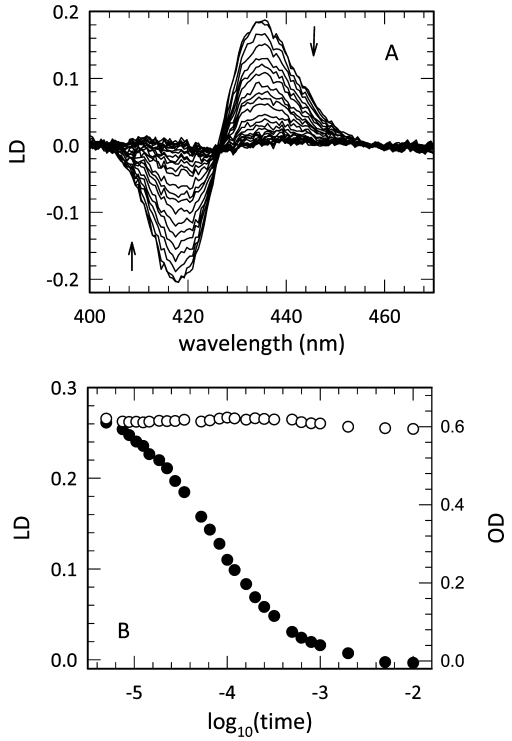

Figure 1. (A) TRLD spectra of MbCO in 50 mM NaP and 300 mg/mL BSA, pH 7. These data represent a typical set of TRLD spectra obtained after photolysis of MbCO. The arrows indicate the direction of the LD change at the 418 nm minimum and the 434 nm maximum bands. (B) Comparison of the peak-to-trough amplitudes calculated from TROD and TRLD data sets for 400 mg/mL BSA. The black symbols represent the peak-to-trough amplitudes for the TRLD data, whereas the white symbols show the corresponding TROD data.

RESULTS

Figure 1A shows a typical set of TRLD spectra measured after photolysis of MbCO. In this case, MbCO is in the presence of 50 mM NaP and 300 mg/mL BSA (pH 7). The spectra shown were collected at 27 time points from 2.5 ns to 10 μs after photolysis of the heme-CO ligand. Using SVD and global kinetic analysis, the data were best fit to two exponential processes with lifetimes of 4.9 ± 0.7 and 92 ± 5 ns. Rotational diffusion of MbCO following photolysis is assigned to the second exponential process, whereas the first exponential lifetime is attributed to distortion of the earliest TRLD data because the laser pulse extends over several nanoseconds. This early exponential process is not affected by concentration, molecular weight, or size of the cosolvent. Figure 1B compares the peak-to-trough amplitudes for the TROD (white symbols) and TRLD (black symbols) data as a function of time following photolysis of MbCO in 400 mg/mL BSA (pH 7). Whereas the TRLD signal returns to zero by 10 μs, the TROD signal remains constant, demonstrating that the TRLD data report rotational diffusion processes that are not compromised by the ligand rebinding reaction.

Figures 2 and 3 show the results of the TRLD measurements (rotational lifetimes) as a function of sucrose and inert macromolecular crowder concentration (w/v %), as well as the normalized residuals for both exponential and linear fits to the data (see also Table 1). The linear fits are divided into different regions by the fitting procedure described above. Transition (or critical[43]) concentrations determined from these

DOI: 10.1021/acs.jpcb.7b04107
J. Phys. Chem. B 2017, 121, 7064−7074

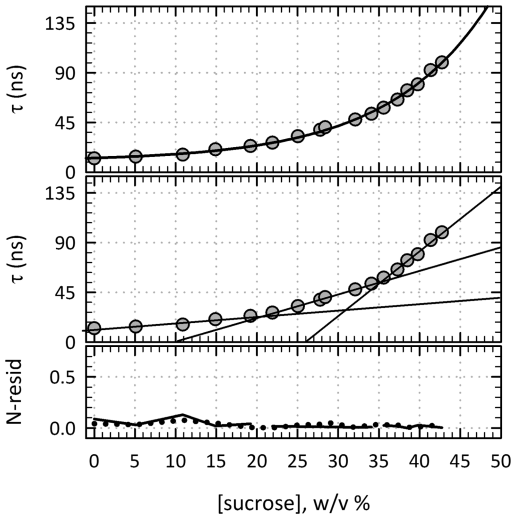

Figure 2. Exponential versus linear fits to the w/v % concentration dependent TRLD data measured for sucrose. The three graphs show the changes in the rotational diffusion time (gray circle) as a function of cosolvent concentration along with the exponential fit (top panel) and the linear fits (middle panel). The normalized residuals for the exponential (dotted line) and linear (black line) fits are shown in the bottom panel. The exponential and linear equations that fit the data are summarized in Table 1.

plots are 21% and 37% for D70, 21% and 37% for D10, 29% and 42% for D6, 26% and 43% for F70, and 21% and 35% for sucrose. The transition concentrations for the macro- and microviscosities of the various macromolecular solutions studied here are summarized in Table S2. A visual comparison of the residuals shows that the sucrose and the dextran data can be fit reasonably well to both linear and exponential functions. The average normalized residuals for the exponential/linear fits for D70, D10, D6, F70, and sucrose are 0.066/0.068, 0.058/0.07, 0.086/0.04, 0.15/0.07, and 0.028/0.029, respectively. These numbers correspond to a 3%, 17%, and 4% improvement in residuals for the exponential versus the linear fits of D70, D10, and sucrose. In contrast, the residuals for the linear fits of the D6 and F70 data are both improved by about 50% over the exponential fits.

Similarly, Figure 4 shows the BSA concentration (w/v %) dependence of the τ measured by TRLD as a function of pH. The TRLD data are shown with the exponential and linear fits, as well as the normalized residuals. As with the inert crowders, the TRLD data for BSA measured at pH 6.5 could be fit to three linear sections to give two transition concentrations: 31% and 43%. At pH 7, the TRLD data can only be fit to two linear segments, with a concentration transition at 40%. The significant improvement in residuals (68% for pH 7 and 37% for pH 6.5) shows clearly that the linear fits are better than the exponential fits. The equations used to generate the exponential and linear fits to the inert and protein data are summarized in Table 1.

To understand the viscosity encountered by protein movements in folding and function processes, η (macroviscosity (bulk viscosity)) and μ_η (microviscosity) are compared. Figure 5 shows plots of η and μ_η as a function of cosolvent concentration for sucrose, glycerol, the dextrans, Ficoll, and BSA. In Figure 5A, these plots are compared for sucrose and glycerol, two small cosolvents that are not expected to contribute excluded volume effects to a solution's properties. For both cosolvents, the concentration dependence of the measured η and calculated μ_η overlay (η/μ_η = 1) as expected from the SED prediction. Note that the fits (black and gray solid and dotted lines) to the sucrose and glycerol macro- and microviscosity data in Figure 5A are also shown in Figure 5B–D.

The plots of η and μ_η as a function of dextran concentration show decreases in the macroviscosity from D70 to D10 to D6 (Figure 5B). However, the μ_η's are about the same for the three dextrans. For example, at 30%, η is 185, 25, and 12 cP, respectively, for D70, D10, and D6, whereas the corresponding μ_η's are 5.9, 6, and 5 cP. In Figure 5C, BSA at both pH 7 and 6.5 show similar macro- and microviscosities, as demonstrated by the η and μ_η values for BSA—12.7 and 11.6 cP and 4.7 and 3.5 cP, respectively, at 30% concentration. Figure 5D compares the viscosity data for F70 with that for D70. Although F70 and D70 are molecular weight equivalents, the two macromolecules exhibit different macro- and microviscosities. At 30% concentration, the macroviscosity of D70 solutions (185 cP) is about 9 times that for F70 (20.8 cP). The microviscosity of a F70 solution, however, is only about 1.5 times less (than D70) at 3.8 cP. The exponential fits that describe the behaviors of the micro- and macroviscosities as a function of concentrations for the cosolvents in Figure 5 are summarized in Table S3. The corresponding linear fits are tabulated in Table S4.

To simplify the comparison of microviscosities of different crowders, Figure 6 shows μ_η at select crowder concentrations. At 10%, the μ_η's for the macromolecules cluster between those for sucrose (1.3 cP) and BSA at pH 7 (2.3 cP). All the microviscosities increase slightly at 20%, but still remain within the values for sucrose (1.8 cP) and BSA at pH 7 (3.1 cP). The μ_η's at 30% start to separate between the inert and protein crowders, with the values for D70, D10, and D6 showing no significant MW dependence (5.9, 6, and 5 cP, respectively) and BSA at pH 7 (4.7 cP) still being higher than that at pH 6.5 (3.5 cP). From 10% to 30%, the μ_η values for F70 follow most closely those for BSA at pH 6.5. However, at 40%, μ_η for F70 falls between those for the dextrans and BSA. When the concentration reaches 50%, the inert and protein crowders become distinctly separated, with the microviscosities for the protein crowders clustering close to that for sucrose. μ_η for 50% F70 becomes greater than the value for D6.

Concentration Transitions. Intrinsic viscosity, $[\eta]$, and specific viscosity, η_{sp}, provide information about the physical properties of polymers. Whereas both $[\eta]$ and η_{sp} are governed by the size and conformation of individual polymer molecules, η_{sp} also indicates changes in intermolecular interactions (aggregation, association). $[\eta]$, being an indicator of hydrodynamic volume of isolated polymers, is usually obtained over a low concentration range. When η_{sp} is plotted as a function of reduced concentration ($c[\eta]$), a change in conformation is indicated by a somewhat abrupt change of the macroviscosity. The concentration at this sudden change in macroviscosity has been described as a critical concentration, after which solutions pass into a higher concentration regime. For many polymers, the behavior of η_{sp} is marked by two critical concentrations, c^* and c^{**}, which separate the dilute, semidilute, and concentrated regions.[43−46] Dilute solutions ($c < c^*$) are characterized by crowder molecules that are highly expanded and behave independently of each other. Initial contact between individual molecules triggers the first transition, c^*.[45] The range between c^* and c^{**} is described by counteracting effects of gradual coil contraction, which dominates the early region of this semidilute segment, and increasing entanglement coupling between polymer chains,[45,47] which arises from coil overlap and

DOI: 10.1021/acs.jpcb.7b04107
J. Phys. Chem. B 2017, 121, 7064−7074

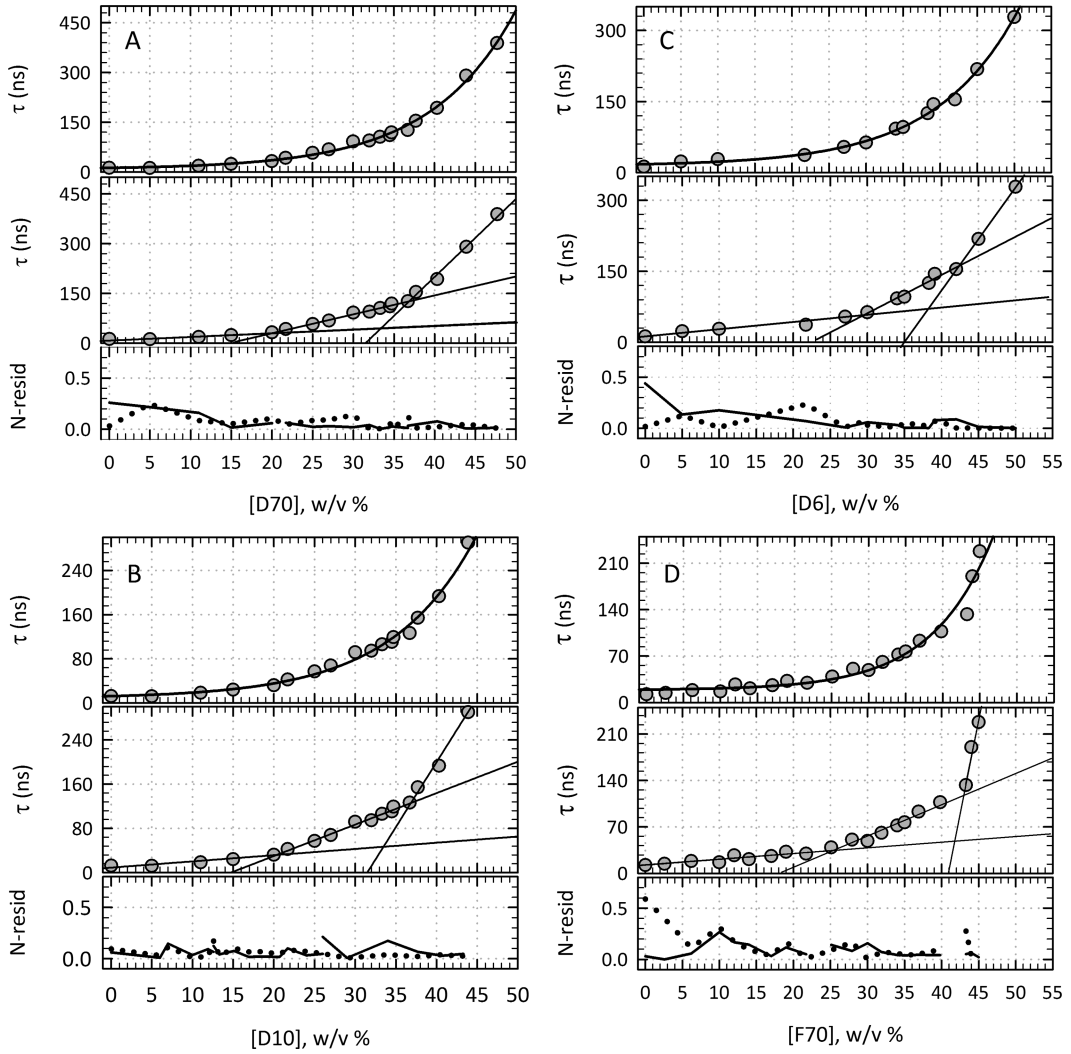

Figure 3. Exponential versus linear fits to the w/v % concentration dependent TRLD data measured for (A) D70, (B) D10, (C) D6, and (D) F70. See Figure 2 legend for details.

interpenetration and dominates in the latter part of this same concentration regime. Initiation of long-range entanglement leads to the second critical concentration, c^{**}, which begins another linear section.[45,46]

Although the focus of this study is on the higher end of concentrations, the linear fits to the concentration dependent τ, η, and μ_η data also show largely three distinct linear regions (Figures 2−4) similar to those observed when η_{sp} is plotted as a function of reduced concentration.[43] Because the concentrations at which the macro- and microviscosities change slope in this study are not obtained in the same way as for the critical concentrations (c^*, c^{**}) determined using η_{sp}, for this study they are called transition concentrations ($c1$ and $c2$) and are denoted $c1(\eta/\eta_o)$ (or $c1(\mu_\eta/\mu_{\eta o})$) and $c2(\eta/\eta_o)$ (or $c2(\mu_\eta/\mu_{\eta o})$) for macroviscosity and microviscosity (μ_η). Table S2 summarizes the $c1$ and $c2$ values obtained from the fits of the linear segments for the concentration vs η/η_o and concentration vs $\mu_\eta/\mu_{\eta o}$ plots (data not shown). Notably, there are only two linear regimes in the concentration versus μ_η plot for pH 7 BSA, whereas all other crowders have three linear sections. It is possible that the outstanding characteristic of BSA at pH 7, its large negative surface charge ($\zeta \sim -12$ mV), plays a role in this significant difference. By comparison, at pH 6.5 (0.1 M $MgCl_2$), the ζ for BSA decreases to about −3 mV. The electrostatic interaction between protein charge and other charges in solution, such as small ions or other proteins, leads to an increase in macroviscosity and is known as the electroviscous effect.[48,49] However, as concentrations increase, the behavior of macroviscosity is governed by intermolecular forces that arise from the close proximity of the molecules. Such intermolecular interactions largely include nonspecific electrostatic, van der Waals, and excluded volume forces, but specific contacts are possible from protein−protein, protein−solvent, and hydrogen bonding interactions.

DISCUSSION

The TRLD determinations of microviscosities, from the measured rotational diffusion lifetimes, provide a valuable method for probing the effects of a crowded environment because (1) the rotational diffusion times obtained from TRLD experiments on MbCO are not compromised by ligand-rebinding chemistry and (2) reorientation of Mb through rotational diffusion occurs on distance and time scales that are close to those expected for early folding/function events.

Relating Crowding-Effected Viscosity to Protein Folding. As intracellular protein/macromolecule concentrations vary, so do viscosities. These two effects influence diffusion, a physical

DOI: 10.1021/acs.jpcb.7b04107
J. Phys. Chem. B 2017, 121, 7064−7074

Table 1. Exponential and Linear Fits to Concentration Dependent TRLD τ

crowder	exponential fits	residuals[a]	linear fits	residuals[b]
Dextran 70	$f = 8.85 + 3.95\exp(0.096x)$	0.066	0−20% | $f = 9.2 + 1.1x$	0.068
			20−37% | $f = -83.6 + 5.7x$	
			37−50% | $f = -738 + 23.4x$	
Dextran 10	$f = 5.5 + 5.7\exp(0.084x)$	0.058	0−24% | $f = 6.59 + 1.49x$	0.07
			24−34% | $f = -93.98 + 5.75x$	
			34−45% | $f = -336.1 + 12.86x$	
Dextran 6	$f = 14.2 + 3.6\exp(0.09x)$	0.086	0−30% | $f = 12.6 + 1.5x$	0.04
			30−40% | $f = -179.8 + 8x$	
			42−50% | $f = -761.1 + 21.8x$	
Ficoll 70	$f = 18.94 + 0.78\exp(0.12x)$	0.15	0−22% | $f = 12.03 + 0.87x$	0.07
			25−40% | $f = -84.8 + 4.7x$	
			43−48% | $f = -2227 + 54.7x$	
BSA, pH 7	$f = 22.6 + 2.8\exp(0.082x)$	0.19	0−40% | $f = 12.9 + 1.8x$	0.06
			40−45% | $f = -382 + 11.7x$	
BSA, pH 6.5	$f = 15.4 + 1.8\exp(0.096x)$	0.079	0−29% | $f = 11.2 + 1.03x$	0.05
			32−43% | $f = -145 + 6.13x$	
			43−48% | $f = -548 + 15.5x$	
Sucrose	$f = 10.1 + 2.8\exp(0.081x)$	0.028	0−19% | $f = 11.3 + 0.6x$	0.029
			19−36% | $f = -20.8 + 2.1x$	
			36−45% | $f = -152.5 + 5.9x$	

[a]Normalized residuals. [b]Normalized residuals averaged across the different linear segments.

parameter that is fundamental to many biological processes such as protein folding, protein−protein interactions, and protein and small solute translocation. The distinction between microviscosity and macroviscosity is important for understanding the diffusion of unfolded proteins toward formation of secondary structure. These movements involve distances that require a similar spatial scale when thinking about viscosity. For low-molecular-weight cosolutes (e.g., sucrose), viscosities are microscopically homogeneous and, therefore, identical to the bulk viscosity. In contrast, high-molecular-weight cosolutes (e.g., F70, D70) form a network of pore-like cavities, which results in microscopic spatial heterogeneities. According to studies by Masuda et al.,[50] if the distance that a particle travels is small compared to the pore size, then that particle is expected to rarely have contact with the crowding cosolute and will exhibit diffusion similar to that when in water. When the diffusional distances are long, the particle's travels can be disrupted by the crowder and the diffusional constant is then expected to be smaller than that for water. Thus, for folding processes that involve large sections of protein structure the local viscosity might be relatively high, but the diffusional formation of protein secondary structure in the inert crowders is expected to be relatively unimpeded, as if in water. In fact, this has been shown to be true for studies of small peptides and a full-length protein.[13,24,51] At least, such an outcome can be expected for certain concentrations of inert macromolecular crowders, as discussed below. With protein crowders, other contributing factors, particularly electrostatic interactions, are anticipated.

Microviscosity Measured by TRLD. A comparison of macroviscosity with the calculated microviscosity gives a measure of how much the viscosity experienced by a probe protein deviates from the inversely proportional relationship between diffusion and viscosity (SED prediction). For small cosolvents sucrose and glycerol, their respective macro- and microviscosities agree (Figure 5A), but deviations arise with increasing cosolvent size. As expected, with increasing concentrations the microviscosities for all macromolecular crowders studied here showed departure from their respective macroviscosities (Figure 5A−C).

The results of previous studies of probe diffusion through solutions of varying concentrations and molecular weights of dextran have been plotted in different ways and fit to different functions, such as linear, exponential, stretched exponential, and power-law, or a combination.[12,34,52−54] With the exception of D70, most of the investigations referenced used largely higher MW dextrans (up to 2000 kDa) and focused on lower concentrations (up to 20 mg/mL) than the experimental parameters studied here. For example, Turner et al. studied diffusion (D/D_0) of polystyrene spheres through solutions of dextran using quasi-elastic light scattering.[53] The dextran MW's used ranged from 20 to 2000 kDa at concentrations up to 20 mg/mL. Research by Phillies et al. used polystyrene latex spheres to probe diffusion (D/D_0) in dextrans of MW 20, 40, 70, 110, and 500 kDa at concentrations as high as 250 mg/mL.[54] For both these studies, as well as for the experiments here, a linear relationship was observed for the dextran concentrations below 20 mg/mL. Once the concentrations reached 250 mg/mL, Phillies et al. report that the data are better fit to stretched exponentials.

The concentrations of most of the macromolecules studied here reached nearly 500 mg/mL. Such a high concentration allows understanding of intracellular crowding that may be present in such environments as the mitochondrial matrix and is considerably higher than the average high concentration of 250−350 mg/mL for most other studies. Here, the concentration-dependent rotational diffusion time (proportional to μ_η) data for D70, D10, and D6 can be fit well to simple exponential functions (Figure 3). (A comparison of the TRLD results with those from the groups of Visser and Waxham is presented in the SI.) That stretched exponential functions are not necessary for a good fit to the data is supported by FCS studies, which used a calmodulin-labeled-with-enhanced-green-fluorescent-protein (eGFP-CaM) probe to follow viscosity (η/η_o) as a function of concentrations as high as 30% dextrans that have MW's of 70, 150, 250, and 500 kDa.[12] Only for dextran 250 kDa was the fit slightly better with a stretched exponential. Whereas the dextran data reported

DOI: 10.1021/acs.jpcb.7b04107
J. Phys. Chem. B 2017, 121, 7064−7074

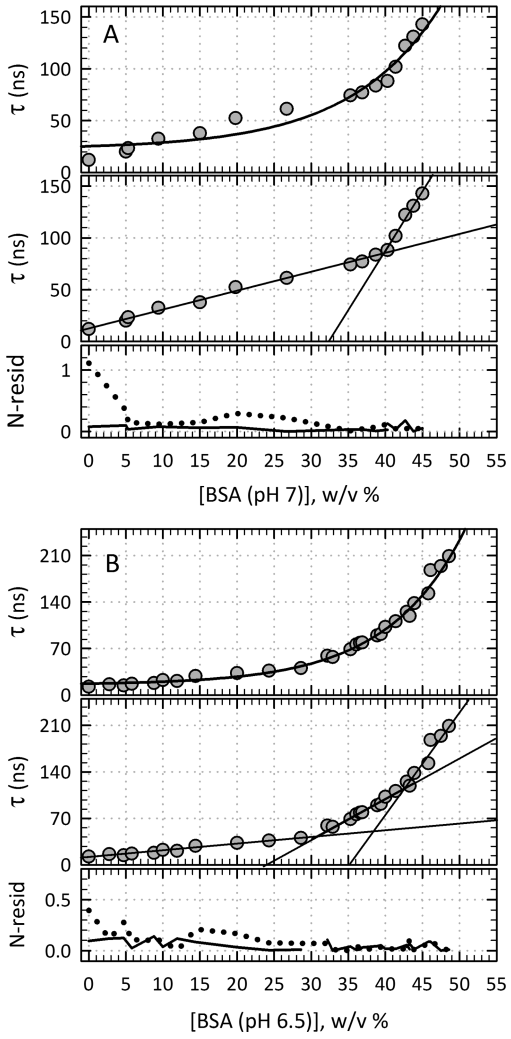

Figure 4. Exponential versus linear fits to the w/v % concentration dependent TRLD data measured for (A) BSA pH 7 and (B) BSA, 0.1 M $MgCl_2$ (pH 6.5). Details in Figure 2 legend.

here are nicely fit to simple exponential functions, they can also be fit to a set of linear functions with similar normalized residuals. In contrast, the residuals are significantly improved for the linear fits (versus the fits to exponential functions) to the TRLD data of MbCO in protein crowders (Figures 2–4, Table 1). The improvement of linear fits over exponential fits could suggest several phase transitions which occur at different macromolecular crowder concentrations.

Characteristics of Macromolecular Crowders. To determine how different physical properties (size, shape, MW, and charge) influence solution microviscosity, MbCO samples were prepared with varying concentrations of sucrose, glycerol, D70, D10, D6, F70, and BSA for TRLD measurements. The effect of (1) MW is examined using D70, D10, and D6; (2) shape is investigated by comparing TRLD results for D70 and F70; (3) size is explored using the small cosolvents, the dextrans, and BSA; and (4) charge is studied by measurements with protein crowders.

Shape. The effect of macromolecule shape on protein rotational diffusion is probed by TRLD measurements of Mb in the presence of dextran and Ficoll. Comparison of F70 and D70 (Figure 5B and D) shows that the two inert macromolecules have similar macroviscosities up to about 10%, but then the macroviscosity for D70 increases dramatically, becoming

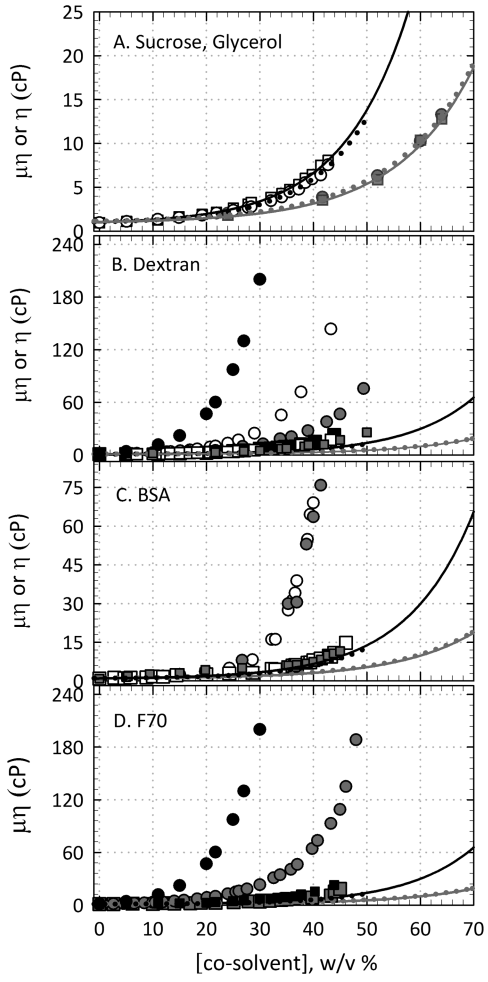

Figure 5. Comparison of the concentration dependent macroviscosity (circles) and microviscosity (squares) data for (A) glycerol (gray symbols) and sucrose (white symbols) and (B) D70 (black symbols), D10 (white symbols), and D6 (gray symbols); (C) BSA at pH 7 (gray symbols) and pH 6.5 (0.1 M $MgCl_2$) (white symbols); and (D) D70 (black symbols) and F70 (gray symbols). The dotted and solid lines in B–D are the fits to the macro- and microviscosity data, respectively, for sucrose (black) and glycerol (gray) that are shown in A.

about 9 and 11 times that for F70 at 30% and 40%. In contrast, the microviscosities are similar for D70 and F70 up to 20%, after which they are only about twice as large at 40% when compared to the values for F70. In fact, at 40% the microviscosity for F70 is more closely aligned with that for D6 and is, in fact, lower and more similar to sucrose than are all dextrans (Figure 6).

Because the MW's of D70 and F70 are the same and they are both considered to be inert under the conditions of this study (vide infra), the difference in shape and deformability may explain the observed microviscosity differences. Dextran is a slightly branched polymer of α-1,6-linked D-glucose units whose structure deviates from linearity (rodlike shape) as MW increases.[55] Between MW's of 2000 and 100 000 (when the macromolecule begins to behave as if it is highly branched), dextrans in water or dilute salt solutions are suggested to be flexible (expandable), near-perfect statistical coiled polymers that undergo little intermolecular interactions, and therefore, do not exhibit association or aggregation.[55] As the concentration increases the polymer coils overlap and interact, leading to aggregation, an effective increase in molecular size, and a very rapid increase in macroviscosity.[43,45−47,56] The flexibility of dextran is demonstrated

DOI: 10.1021/acs.jpcb.7b04107
J. Phys. Chem. B 2017, 121, 7064−7074

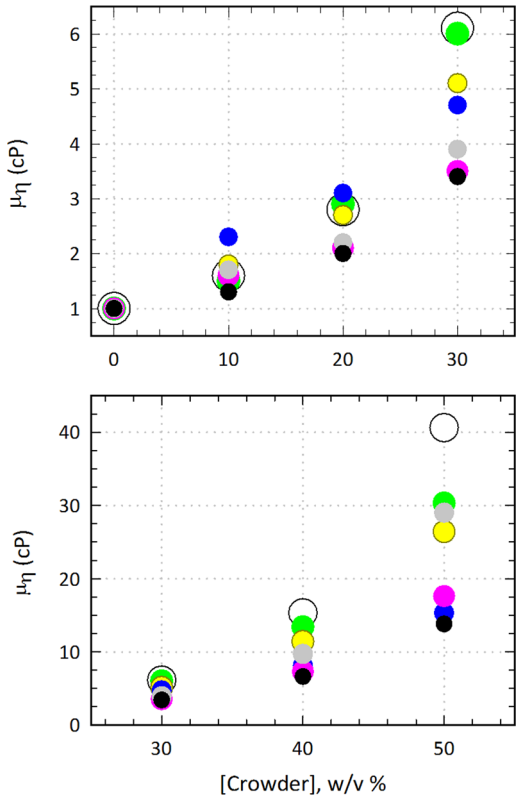

Figure 6. Comparison of the microviscosity data at 10%, 20%, 30%, 40%, and 50% w/v concentration for sucrose (black), D70 (white), D10 (green), D6 (yellow), BSA pH 7 (blue), BSA pH 6.5 (pink), and F70 (gray). The values of μ_η for 50% crowder were calculated from the respective exponential fits to the data. For all other concentrations the μ_η values were obtained from TRLD measurements. The sizes of the symbols are different only for presentation purposes, because some symbols would be buried behind others.

by theoretical studies that indicate considerable conformational freedom in the α-1−6 linkage and by studies of solute diffusivity through membranes of different pore sizes.[57] That dextran was able to diffuse through the membrane pores, even those with smaller diameters than the dextran itself, more readily than the Stokes−Einstein-radius-equivalent Ficoll, suggests that the former has greater conformational mobility.

In contrast to dextran, Ficoll has typically been described and modeled as a rigid and compact hard sphere because it is a highly cross-linked copolymer of sucrose and epichlorohydrin. However, the results of diffusion data characterize Ficoll by strong hydrodynamic interactions and a low-asymmetry shape that lies somewhere between random coil chains and spheres.[58] This deviation from the ideal hard sphere model is supported by size-exclusion chromatography studies that correlate a ∼15% increase in intrinsic viscosity upon switching solution conditions from low (0.0015 M) to physiological (0.1−0.25 M) ionic strength to expansion of Ficoll.[59] Additional support is provided by crowding experiments that probe the fractional volume occupancy (the total volume occupied by all solutes), the intrinsic viscosity, and the calculated covolume (reportedly synonymous with excluded volume) as a function of F70 concentration.[60] Up to a concentration of 2.5%, an increase in excluded volume was observed and attributed to intermolecular interactions between the F70 molecules. However, the decrease in excluded volume between 2.5% and 10% Ficoll 70 was considered to arise from molecular compression or interpenetration. Although the highest concentration (50%) reported in these TRLD studies is five times that examined by Wenner et al.,[60] the microviscosity behavior with increasing F70 concentration in Figures 5D and 6 is consistent with diminished excluded volume, as it follows closely the data for sucrose up to 40%. The outstanding physical characteristics that distinguish Ficoll from dextran macromolecules at lower concentrations are the rather symmetric, open, yet deformable (compressing and interpenetrating) structure that affects excluded volume for the former and the conformationally flexible, noninteracting coiled polymers that is descriptive of the latter. At higher concentrations, the overlapping, interacting polymers with diffusive mobility can explain the higher microviscosity observed for dextran versus Ficoll.

Molecular Weight and Size. By keeping the macromolecules in the dextran family, there is some degree of control over variables that might affect viscosity. Thus, the dependence of macroviscosity and microviscosity on crowder concentration for D70, D10, and D6 was compared to explore how molecular weight affects the rotational diffusion of Mb. As expected, the dependence decreases from D70 to D10 to D6. The differences in microviscosity, as influenced by the molecular weight and size, are most obvious as the dextran concentration increases above 40% (Figure 5).

Comparison of the concentration parameters (Table S2) shows that the protein probe (of microviscosity) observes transitions from dilute to semidilute ($c1(\mu_\eta/\mu_{\eta o})$) and from semidilute to concentrated ($c2(\mu_\eta/\mu_{\eta o})$) conditions in a fashion similar to that for the macroviscosity ($c1(\eta/\eta_o)$ and $c2(\eta/\eta_o)$) when followed with a viscometer. These results suggest that, as expected, there is no interaction between the inert dextran macromolecules and the protein probe. Under dilute solution conditions ($c1(\mu_\eta/\mu_{\eta o})$ and $c1(\eta/\eta_o)$) this result is expected because the macromolecules are not in close or constant contact. On transitioning from semidilute to concentrated solution conditions, the values for $c2(\mu_\eta/\mu_{\eta o})$ and $c2(\eta/\eta_o)$ show a gradual increase in concentration as MW decreases.

Charge. Unlike protein crowders, dextran and Ficoll have generally been classified as inert macromolecules. However, several size exclusion chromatography studies have indicated that Ficoll and dextran have very weak negative charges,[59,61−65] as only a few charges are found per molecule and the existence of the charge is dependent upon pH and ionic strength.[63,64] Under those conditions and for this study, dextran and Ficoll are effectively considered inert and are thus expected to cleanly exert the major crowding effects of excluded volume and viscosity.

Charge, however, can become a significant additional factor that influences viscosity when using protein crowders. The charged groups on a protein align opposite charges in its solution environment to create an "electric double layer" that moves with the protein molecule and thus increases friction.[66] A secondary effect is the intermolecular repulsion between the double layers. If the repulsion influences a shape change of the protein, this is considered a tertiary effect. Together, this electroviscous effect (vide supra) arising from the net charge of the protein plays a significant role in viscosity behavior. However, this is true only in dilute solutions. At high concentration (>200 mg/mL) it is necessary to consider other intermolecular factors such as van der Waals and excluded volume interactions.

Zeta potential, which is related to surface charge, can be used to correlate the TRLD measurements with the effect of charge on microviscosity. At pH 7, BSA has a ζ of about −12 mV.[38,40,42] In the presence of 0.1 M $MgCl_2$ and pH 6.5,

DOI: 10.1021/acs.jpcb.7b04107
J. Phys. Chem. B 2017, 121, 7064−7074

ζ is about −3 mV, which is equivalent to ∼pH 5.2 in the absence of salt.[38,39] The pI of BSA is about pH 5, although it appears to range from 4.8 to 5.6.[38] (See SI for a discussion on previously observed changes in macroviscosity as a function of pH.)

BSA was used to determine how the rotational diffusion time (microviscosity) changes as the surface charge of BSA decreases away from the large ζ value of −12 mV (pH 7) to ∼−3 (pH 6.5, 0.1 M $MgCl_2$), which approaches characteristics more like that of an inert macromolecule. In Figure 6, when microviscosity is plotted as a function of cosolvent concentration, the trace for BSA at pH 6.5 is much closer to that for sucrose than is D70 at concentrations greater than 30%. The microviscosities depart from the macroviscosities at 15−20% higher concentration for BSA (pH 6.5) compared to D70 (Figure 5B,C). The molecular weight is not expected to contribute significantly to this difference because they are approximately the same (66 436 Da and 70 000 Da). However, two outstanding characteristics—the slightly negative charge on BSA (pH 6.5) and the difference in its radius (39 Å) compared with D70 (58 Å)—may contribute.

If surface charge is a major influence on the microviscosities of BSA, then there should be a significant difference in the concentration versus microviscosity plots for BSA at pH 7 versus pH 6.5. As it turns out, the 7-fold larger surface charge at pH 7 leads to 50−70% higher microviscosity from 10% to 35% BSA, but then becomes 10% to 30% lower from 40% to 55% BSA when compared to the values for BSA at pH 6.5 (Figure 6). Up to 20% BSA (pH 7), the microviscosities are larger than for both BSA at pH 6.5 and D70. However, at concentrations from 30% to 50%, the microviscosities for D70 become significantly larger than for the BSA's. This increase in D70 microviscosity is due to the gradual entanglement as the concentration increases. When the negatively charged BSA molecules are in close proximity (high concentrations) the electrostatic interparticle repulsion is expected to push the molecules apart and decrease viscosity. With a smaller negative surface charge for BSA at pH 6.5 (0.1 M $MgCl_2$), and therefore, lower electrostatic repulsion, the microviscosities are greater than at pH 7. Another consequence of like-charged molecular interactions is that the electrostatic repulsions decrease aggregation. Consequently, it would take higher concentrations to facilitate aggregation of the protein. This effect may explain why the transition concentrations (Table S2) are higher for the BSAs than the dextrans. With a smaller ζ there is weaker electrostatic repulsion, making it easier for aggregation to play a more significant role at higher concentration. This result is consistent with the expectation that when the solution conditions are adjusted to decrease surface charge the protein macromolecule will start to behave more like an inert crowder (e.g., as ζ approaches 0 or pH approaches pI). (See SI for a comparison of the BSA results in this study with previous studies of BSA macroviscosity.) The possibility of probe Mb interacting with the protein crowders is considered unlikely given that the macroviscosities and microviscosities, measured by different approaches, have similar transition concentrations.

Extrapolation to the Cell. The intention of this study is to measure microviscosities of crowded solutions, such as those used in studies of protein folding, and to provide useful equations that allow calculation of microviscosities of these solutions. To understand how relevant these microviscosity measurements are to intracellular environments, these results are discussed in the context of studies that measure viscosity in cells. This, however, is not trivial because many studies of cellular viscosities (microviscosities) have reported a large range of results that likely arise from differences in the kind of probe and the kind of diffusion (rotational versus translational) followed by that probe. There are the added factors of the spatial location (mitochondrial matrix, cytoplasm, etc.) and the temporal phase of the cell cycle that is being monitored, as well as the fact that cells have multiple types of macromolecules. Thus, only qualitative comparison of viscosities measured with TRLD and macromolecular crowders and of viscosities measured in cells is approached—by using the cellular concentrations of macromolecules reported in the literature and the equations determined in this study to calculate microviscosities. Those microviscosities will then be compared with literature values for viscosities measured in the cell using similar rotational diffusion probes (Table S5).

Two cellular locations are considered—cytoplasm and mitochondrion—because they are expected to have distinctly different viscosities and macromolecular concentrations. For the cytoplasm, protein concentrations that range from 180 to 440 mg/mL have been reported for *E. coli* K-12 strain MG1655, HeLa, and *E. coli* HEK293 cells.[67−69] At the low end, these concentrations translate to microviscosities of about 2 to 3 cP calculated with the equations from Table S3 for all the crowder macromolecules used in this study, and of about 10 to 21 cP at 440 mg/mL. Within this 2 to 21 cP microviscosity range, studies have reported about 1−13 cP viscosity values from measurements in J774 microphage, Swiss 3T3 fibroblasts, Chinese Hamster lung cells V79, and MDCK cells, which correspond to calculated concentrations of <10 mg/mL to as high as 480 mg/mL.[22,70−74] If a solution of F70 alone has a measured viscosity of 3.5 cP, then the calculated concentration of 287 mg/mL is quite close to the cytoplasmic measurement of 275 mg/mL. For BSA at pH 7, with a measured concentration of 440 mg/mL, the calculated μ_η is 10.3 cP and is consistent with the *in situ* measurement of 10 cP.

In harvested rat livers, fluorescence anisotropy measurements indicate viscosities that are 25 and 37 times more viscous than water in the orthodox versus condensed configuration of the mitochondria, with protein concentrations of 260 and 560 mg/mL, respectively.[4,28] The calculated microviscosities for 560 mg/mL range from 23 to 69 cP for the macromolecular crowders. A fluorescence anisotropy measurement of 37 cP[28] corresponds to calculated concentrations of 490 to 630 mg/mL for an average of about 560 mg/mL. For a solution of BSA at pH 6.5 having a μ_η of 37 cP, the calculated concentration of 578 mg/mL is very close to the measured 560 mg/mL.

The consistency between the results of the calculated (from Table S3) μ_η's and concentrations and the reported literature values for both parameters is striking in light of at least two major concerns. First, there is contrasting heterogeneity and homogeneity of the respective cellular and *in vitro* environments. Most distinctly, cellular microviscosities are expected to change as a function of probe location in the cell. Second, the studies used for comparison with the TRLD results monitor microviscosity with probes of different sizes and nature (proteins versus fluorescent dyes). However, the differences in probe sizes are secondary to the fact that the data compared are all based on studies that also monitor rotational diffusion. Because it seems that many more studies monitor microviscosities through translational diffusion, it is important that the same type of diffusion is considered. That there is close

DOI: 10.1021/acs.jpcb.7b04107
J. Phys. Chem. B 2017, 121, 7064−7074

agreement of the measurements suggests that this approach may be broadly applicable to the study of rotational diffusion in crowded environments.

■ ASSOCIATED CONTENT

Supporting Information

The Supporting Information is available free of charge on the ACS Publications website at DOI: 10.1021/acs.jpcb.7b04107.

Comparison of TRLD-determined microviscosities with previous studies; Additional tables—crowder properties, transition concentrations, exponential and linear fits to concentration dependence of macro- and microviscosity, and extrapolations to the cell (PDF)

■ AUTHOR INFORMATION

Corresponding Author

*E-mail: kliger@ucsc.edu. Phone: 831.459.2106. Fax: 831.459.2935.

ORCID

Eefei Chen: 0000-0001-7411-7779

Notes

The authors declare no competing financial interest.

■ ACKNOWLEDGMENTS

We thank Pernilla Wittung-Stafshede, Robert Goldbeck, and Raymond Esquerra for helpful discussions and suggestions.

■ ABBREVIATIONS

LD, linear dichroism; TRLD, time-resolved linear dichroism; Mb, myoglobin; MbCO, carbonmonoxy myoglobin; BSA, bovine serum albumin; D6, dextran 6000; D10, dextran 10 000; D70, dextran 70 000; F70, Ficoll 70 000; SED, Stokes−Einstein Debye; SVD, singular value decomposition

■ REFERENCES

(1) Silverman, L.; Glick, D. Measurement of protein concentration by quantitative electron microscopy. *J. Cell Biol.* **1969**, *40* (3), 773−8.

(2) Ellis, R. J. Macromolecular crowding: an important but neglected aspect of the intracellular environment. *Curr. Opin. Struct. Biol.* **2001**, *11* (1), 114−9.

(3) Okutucu, B.; Dincer, A.; Habib, O.; Zihnioglu, F. Comparison of five methods for determination of total plasma protein concentration. *J. Biochem. Biophys. Methods* **2007**, *70* (5), 709−11.

(4) Hackenbrock, C. R. Chemical and physical fixation of isolated mitochondria in low-energy and high-energy states. *Proc. Natl. Acad. Sci. U. S. A.* **1968**, *61* (2), 598−605.

(5) Ralston, G. B. Effects of crowding in protein solutions. *J. Chem. Educ.* **1990**, *67* (10), 857−860.

(6) Minton, A. P. Influence of macromolecular crowding upon the stability and state of association of proteins: predictions and observations. *J. Pharm. Sci.* **2005**, *94* (8), 1668−75.

(7) Zimmerman, S. B.; Minton, A. P. Macromolecular crowding - biochemical, biophysical, and physiological consequences. *Annu. Rev. Biophys. Biomol. Struct.* **1993**, *22*, 27−65.

(8) Wang, D.; Kreutzer, U.; Chung, Y. R.; Jue, T. Myoglobin and hemoglobin rotational diffusion in the cell. *Biophys. J.* **1997**, *73* (5), 2764−2770.

(9) Herrmann, A.; Muller, P. Correlation of the internal microviscosity of human erythrocytes to the cell volume and the viscosity of hemoglobin solutions. *Biochim. Biophys. Acta, Mol. Cell Res.* **1986**, *885* (1), 80−7.

(10) Endre, Z. H.; Chapman, B. E.; Kuchel, P. W. Intra-erythrocyte microviscosity and diffusion of specifically labelled [glycyl-alpha-13C]glutathione by using 13C N.M.R. *Biochem. J.* **1983**, *216* (3), 655−60.

(11) Gennaro, A. M.; Luquita, A.; Rasia, M. Comparison between internal microviscosity of low-density erythrocytes and the microviscosity of hemoglobin solutions: an electron paramagnetic resonance study. *Biophys. J.* **1996**, *71* (1), 389−93.

(12) Goins, A. B.; Sanabria, H.; Waxham, M. N. Macromolecular crowding and size effects on probe microviscosity. *Biophys. J.* **2008**, *95* (11), 5362−73.

(13) Mukherjee, S.; Waegele, M. M.; Chowdhury, P.; Guo, L.; Gai, F. Effect of macromolecular crowding on protein folding dynamics at the secondary structure level. *J. Mol. Biol.* **2009**, *393* (1), 227−36.

(14) Wang, Y.; Li, C.; Pielak, G. J. Effects of proteins on protein diffusion. *J. Am. Chem. Soc.* **2010**, *132* (27), 9392−7.

(15) Haidekker, M. A.; Theodorakis, E. A. Environment-sensitive behavior of fluorescent molecular rotors. *J. Biol. Eng.* **2010**, *4*, 11.

(16) Srere, P. A. The Infrastructure of the mitochondrial matrix. *Trends Biochem. Sci.* **1980**, *5* (5), 120−121.

(17) Srere, P. A. The structure of the mitochondrial inner membrane matrix compartment. *Trends Biochem. Sci.* **1982**, *7* (10), 375−378.

(18) Haggie, P. M.; Brindle, K. M. Mitochondrial citrate synthase is immobilized in vivo. *J. Biol. Chem.* **1999**, *274* (7), 3941−5.

(19) Partikian, A.; Olveczky, B.; Swaminathan, R.; Li, Y.; Verkman, A. S. Rapid diffusion of green fluorescent protein in the mitochondrial matrix. *J. Cell Biol.* **1998**, *140* (4), 821−9.

(20) Dieteren, C. E.; Gielen, S. C.; Nijtmans, L. G.; Smeitink, J. A.; Swarts, H. G.; Brock, R.; Willems, P. H.; Koopman, W. J. Solute diffusion is hindered in the mitochondrial matrix. *Proc. Natl. Acad. Sci. U. S. A.* **2011**, *108* (21), 8657−62.

(21) Swaminathan, R.; Hoang, C. P.; Verkman, A. S. Photobleaching recovery and anisotropy decay of green fluorescent protein GFP-S65T in solution and cells: cytoplasmic viscosity probed by green fluorescent protein translational and rotational diffusion. *Biophys. J.* **1997**, *72* (4), 1900−7.

(22) Fushimi, K.; Verkman, A. S. Low viscosity in the aqueous domain of cell cytoplasm measured by picosecond polarization microfluorimetry. *J. Cell Biol.* **1991**, *112* (4), 719−25.

(23) Luby-Phelps, K. Cytoarchitecture and physical properties of cytoplasm: volume, viscosity, diffusion, intracellular surface area. *Int. Rev. Cytol.* **1999**, *192*, 189−221.

(24) Dhar, A.; Ebbinghaus, S.; Shen, Z.; Mishra, T.; Gruebele, M. The diffusion coefficient for PGK folding in eukaryotic cells. *Biophys. J.* **2010**, *99* (9), L69−71.

(25) Ebbinghaus, S.; Dhar, A.; McDonald, J. D.; Gruebele, M. Protein folding stability and dynamics imaged in a living cell. *Nat. Methods* **2010**, *7* (4), 319−23.

(26) Ebbinghaus, S.; Gruebele, M. Protein folding landscapes in the living cell. *J. Phys. Chem. Lett.* **2011**, *2* (4), 314−319.

(27) Dix, J. A.; Verkman, A. S. Mapping of fluorescence anisotropy in living cells by ratio imaging. Application to cytoplasmic viscosity. *Biophys. J.* **1990**, *57* (2), 231−40.

(28) Scalettar, B. A.; Abney, J. R.; Hackenbrock, C. R. Dynamics, structure, and function are coupled in the mitochondrial matrix. *Proc. Natl. Acad. Sci. U. S. A.* **1991**, *88* (18), 8057−61.

(29) Lopez-Beltran, E. A.; Mate, M. J.; Cerdan, S. Dynamics and environment of mitochondrial water as detected by 1H NMR. *J. Biol. Chem.* **1996**, *271* (18), 10648−53.

(30) Liu, T.; Liu, X.; Spring, D. R.; Qian, X.; Cui, J.; Xu, Z. Quantitatively mapping cellular viscosity with detailed organelle information via a designed PET fluorescent probe. *Sci. Rep.* **2015**, *4*, 5418.

(31) Albrecht, A. C. Polarizations and assignments of transitions - Method of photoselection. *J. Mol. Spectrosc.* **1961**, *6* (1), 84.

(32) Che, D. P.; Shapiro, D. B.; Esquerra, R. M.; Kliger, D. S. Ultrasensitive time-resolved linear dichroism spectral measurements using near-crossed linear polarizers. *Chem. Phys. Lett.* **1994**, *224* (1−2), 145−154.

DOI: 10.1021/acs.jpcb.7b04107
J. Phys. Chem. B 2017, 121, 7064−7074

(33) Zhang, C. F.; Farrens, D. L.; Bjorling, S. C.; Song, P. S.; Kliger, D. S. Time-resolved absorption studies of native etiolated oat phytochrome. *J. Am. Chem. Soc.* **1992**, *114* (12), 4569−4580.
(34) Lavalette, D.; Hink, M. A.; Tourbez, M.; Tetreau, C.; Visser, A. J. Proteins as micro viscosimeters: Brownian motion revisited. *Eur. Biophys. J.* **2006**, *35* (6), 517−22.
(35) de Belder, A. N. Dextran. *Dextran Handbook Amersham Sciences* **2003**, 9−14.
(36) Schultz, S. G.; Solomon, A. K. Determination of the effective hydrodynamic radii of small molecules by viscometry. *J. Gen. Physiol.* **1961**, *44*, 1189−99.
(37) Ekemezie, P. M.; Nwadiogbu, J. O.; Enekwechi, E. E. Determination of the diffusion coefficient of sucrose in water and its hydrodynamic radius. *Der Pharma Chemica* **2015**, *7* (6), 1−7.
(38) Yadav, S.; Shire, S. J.; Kalonia, D. S. Viscosity analysis of high concentration bovine serum albumin aqueous solutions. *Pharm. Res.* **2011**, *28* (8), 1973−83.
(39) Salgin, S.; Salgin, U.; Bahadir, S. Zeta potentials and isoelectric points of biomolecules: The effects of ion types and ionic strengths. *Int. J. Electrochem. Sci.* **2012**, *7* (12), 12404−12414.
(40) Matulis, D.; Lovrien, R. 1-anilino-8-naphthalene sulfonate anion-protein binding depends primarily on ion pair formation. *Biophys. J.* **1998**, *74* (1), 422−429.
(41) Zhang, F. J.; Skoda, M. W. A.; Jacobs, R. M. J.; Martin, R. A.; Martin, C. M.; Schreiber, F. Protein interactions studied by SAXS: Effect of ionic strength and protein concentration for BSA in aqueous solutions. *J. Phys. Chem. B* **2007**, *111* (1), 251−259.
(42) Tanford, C.; Buzzell, J. G. The Viscosity of aqueous solutions of bovine serum albumin between pH 4.3 and 10.5. *J. Phys. Chem.* **1956**, *60* (2), 225−231.
(43) Morris, E. R.; Cutler, A. N.; Ross-Murphy, S. B.; Rees, D. A.; Price, J. Concentration and shear rate dependence of viscosity in random coil polysaccharide solutions. *Carbohydr. Polym.* **1981**, *1*, 5−21.
(44) de Gennes, P. G. Brownian motions of flexible polymer chains. *Nature* **1979**, *282* (5737), 367−370.
(45) Kasapis, S.; Morris, E. R.; Gross, M.; Rudolph, K. Solution properties of levan polysaccharide from *Pseudomonas-Syringae* pv *Phaseolicola*, and its possible primary role as a blocker of recognition during pathogenesis. *Carbohydr. Polym.* **1994**, *23* (1), 55−64.
(46) Ioan, C. E.; Aberle, T.; Burchard, W. Light scattering and viscosity behavior of dextran in semidilute solution. *Macromolecules* **2001**, *34* (2), 326−336.
(47) Lefebvre, J. Viscosity of concentrated protein solutions. *Rheol. Acta* **1982**, *21* (4−5), 620−625.
(48) Smoluchowski, M. V. Drei vortrage uber diffusion, Brownsche bewegung und koagulation von kolloidteilchen. *Phys. Zeit.* **1916**, *17*, 557−585.
(49) Komatsubara, M.; Suzuki, K.; Nakajima, H.; Wada, Y. Electroviscous effect of lysozyme in aqueous-solutions. *Biopolymers* **1973**, *12* (8), 1741−1746.
(50) Masuda, A.; Ushida, K.; Nishimura, G.; Kinjo, M.; Tamura, M.; Koshino, H.; Yamashita, K.; Kluge, T. Experimental evidence of distance-dependent diffusion coefficients of a globular protein observed in polymer aqueous solution forming a network structure on nanometer scale. *J. Chem. Phys.* **2004**, *121* (21), 10787−93.
(51) Chen, E.; Christiansen, A.; Wang, Q.; Cheung, M. S.; Kliger, D. S.; Wittung-Stafshede, P. Effects of macromolecular crowding on burst phase kinetics of cytochrome c folding. *Biochemistry* **2012**, *51* (49), 9836−45.
(52) Furukawa, R.; Arauzlara, J. L.; Ware, B. R. Self-diffusion and probe diffusion in dilute and semidilute qqueous-solutions of dextran. *Macromolecules* **1991**, *24* (2), 599−605.
(53) Turner, D. N.; Hallett, F. R. A study of the diffusion of compact particles in polymer solutions using quasi-elastic light scattering. *Biochim. Biophys. Acta, Gen. Subj.* **1976**, *451* (1), 305−12.
(54) Phillies, G. D. J.; Gong, J. J.; Li, L. Y.; Rau, A.; Zhang, K.; Yu, L. P.; Rollings, J. Macroparticle diffusion in dextran solutions. *J. Phys. Chem.* **1989**, *93* (16), 6219−6223.
(55) Basedow, A. M.; Ebert, K. H. Production, characterization, and solution properties of dextran fractions of narrow molecular-weight distributions. *J. Polym. Sci., Polym. Symp.* **1979**, *66*, 101−115.
(56) Fedin, E. I.; Tsitsishvili, V. G.; Grinberg, V. Y.; Bakari, T. I.; Tolstoguzov, V. B. Study of dextran hydration in dilute, aqueous-solution by proton magnetic-relaxation method. *Carbohydr. Res.* **1975**, *39* (2), 193−199.
(57) Bohrer, M. P.; Patterson, G. D.; Carroll, P. J. Hindered diffusion of dextran and Ficoll in microporous membranes. *Macromolecules* **1984**, *17* (6), 1170−1173.
(58) Lavrenko, P. N.; Mikriukova, O. I.; Okatova, O. V. On the separation ability of various Ficoll gradient solutions in zonal centrifugation. *Anal. Biochem.* **1987**, *166* (2), 287−97.
(59) Shah, G.; Dubin, P. L. Adsorptive interaction of Ficoll standards with porous-glass size-exclusion chromatography columns. *J. Chromatogr A* **1995**, *693* (2), 197−203.
(60) Wenner, J. R.; Bloomfield, V. A. Crowding effects on EcoRV kinetics and binding. *Biophys. J.* **1999**, *77* (6), 3234−3241.
(61) Omorodion, S. N. E.; Hamielec, A. E.; Brash, J. L. Optimization of peak separation and broadening in aqueous gel-permeation chromatography (Gpc) - dextrans. *J. Liq. Chromatogr.* **1981**, *4* (1), 41−50.
(62) Kato, Y.; Matsuda, T.; Hashimoto, T. New gel-permeation column for the separation of water-soluble polymers. *J. Chromatogr.* **1985**, *332* (Sep), 39−46.
(63) Porsch, B.; Sundelof, L. O. Size-exclusion chromatography and dynamic light-scattering of dextrans in water - explanation of Ion-Exclusion Behavior. *J. Chromatogr A* **1994**, *669* (1−2), 21−30.
(64) Wang, Y. F.; Dubin, P. L. Observation of ficoll charge using size-exclusion chromatography. *J. Chromatogr A* **1998**, *800* (2), 181−185.
(65) Barth, H. G. A practical approach to steric exclusion chromatography of water-soluble polymers. *J. Chromatogr. Sci.* **1980**, *18* (9), 409−429.
(66) Booth, F. The electroviscous effect for suspensions of solid spherical particles. *Proc. R. Soc. London, Ser. A* **1950**, *203* (1075), 533−551.
(67) Cayley, S.; Lewis, B. A.; Guttman, H. J.; Record, M. T. Characterization of the cytoplasm of *Escherichia-Coli-K-12* as a function of external osmolarity - Implications for protein DNA interactions invivo. *J. Mol. Biol.* **1991**, *222* (2), 281−300.
(68) Boersma, A. J.; Zuhorn, I. S.; Poolman, B. A sensor for quantification of macromolecular crowding in living cells. *Nat. Methods* **2015**, *12* (3), 227.
(69) Pliss, A.; Peng, X.; Liu, L. X.; Kuzmin, A.; Wang, Y.; Qu, J. L.; Li, Y.; Prasad, P. N. Single Cell Assay for Molecular Diagnostics and Medicine: monitoring intracellular concentrations of macromolecules by two-photon fluorescence lifetime imaging. *Theranostics* **2015**, *5* (9), 919−930.
(70) Parker, W. C.; Chakraborty, N.; Vrikkis, R.; Elliott, G.; Smith, S.; Moyer, P. J. High-resolution intracellular viscosity measurement using time-dependent fluorescence anisotropy. *Opt. Express* **2010**, *18* (16), 16607−16617.
(71) Lepock, J. R.; Cheng, K. H.; Campbell, S. D.; Kruuv, J. Rotational diffusion of TEMPONE in the cytoplasm of Chinese-hamster lung-cells. *Biophys. J.* **1983**, *44* (3), 405−412.
(72) Mastro, A. M.; Babich, M. A.; Taylor, W. D.; Keith, A. D. Diffusion of a small molecule in the cytoplasm of mammalian-cells. *Proc. Natl. Acad. Sci. U. S. A.* **1984**, *81* (11), 3414−3418.
(73) Bicknese, S.; Periasamy, N.; Shohet, S. B.; Verkman, A. S. Cytoplasmic viscosity near the cell plasma-membrane - measurement by evanescent field frequency-domain Microfluorimetry. *Biophys. J.* **1993**, *65* (3), 1272−1282.
(74) Dix, J. A.; Verkman, A. S. Crowding effects on diffusion in solutions and cells. *Annu. Rev. Biophys.* **2008**, *37*, 247−263.

DOI: 10.1021/acs.jpcb.7b04107
J. Phys. Chem. B 2017, 121, 7064−7074